ELSEVIER

Journal of Electrostatics 54 (2002) 321–332

Journal of
ELECTROSTATICS

www.elsevier.com/locate/elstat

Electrostatic micromirrors for subaperturing in an adaptive optics system

Mark N. Horenstein[a,*], Seth Pappas[a], Asaf Fishov[a], Thomas G. Bifano[b]

[a] Department of Electrical and Computer Engineering, Boston University, 44 Cummington St., Boston, MA 02215, USA

[b] Department of Manufacturing Engineering, Boston University, 44 Cummington St., Boston, MA 02215, USA

Received 4 August 2000; received in revised form 24 March 2001; accepted 31 March 2001

Abstract

An electrostatic digital mirror device has been used to replace the lenslet array in a simple adaptive optics system. Clusters of binary pixels define the subapertures of the image plane and direct a small portion of the image onto a detector. The detector measures position shifts in the focused subaperture image caused by optical aberrations. Measurements on a digital mirror-based system and a similar lenslet-based system compare favorably to within a simple scaling factor. A subaperture system designed around a digital mirror device could aid in the development of a sequential subaperturing method that would replace the more complex schemes used in traditional adaptive optics. © 2002 Elsevier Science B.V. All rights reserved.

Keywords: Adaptive optics; Micro-electromechanical; MEMS; Electrostatic actuators; Shack–Hartmann

1. Introduction

This paper presents an interesting application of electrostatics and micro-electromechanical systems (MEMS) to the field of optics and wavefront sensing. Wavefront sensors are used in many applications involving medical and terrestrial imaging, target recognition, laser tracking, and astronomical observations. Under ideal conditions, the light emanating from an image source arrives as a series of

*Corresponding author. Tel.: +1-617-353-9052; fax: +1-617-353-6440.
E-mail address: mnh@bu.edu (M.N. Horenstein).

0304-3886/02/$ - see front matter © 2002 Elsevier Science B.V. All rights reserved.
PII: S0304-3886(01)00159-0

uniform wavefronts that behave locally as a plane wave at the image receiving plane. In practice, the image plane can be a camera lens aperture, the human eye, a charge-coupled-device (CCD) array, a photographic plate, or an infrared detector. If the light passes through a distorting medium, it will no longer have the form of a local plane wave at the image plane. Rather, it will appear as a series of non-planar, or "aberrated," wavefronts. In the field of optics, a wavefront sensor can help determine the degree of distortion of the aberrated wave. If the distorted wavefront is modeled as a collection of piecewise-linear wavefront sectors, then the sensor can provide information about the direction of propagation of each sector, and hence the degree to which the aberrated wavefront departs from an ideal plane wave.

Wavefront sensors are extremely important in the field of *adaptive optics* (AO). In an AO system, information about propagation distortion is passed to an image correction device which compensates for media-induced aberrations [1–8]. Examples of image correction devices include electrostatic deformable mirrors [8–16] and liquid crystal phase modulators [4–7]. These devices act to redirect the individual sectors of the incoming wave until they regain their undistorted, planar-wavefront shapes. A beam splitter is used to deflect part of the incoming image onto the wavefront sensor which, in turn, provides correction information to the correction device.

2. The lenslet array

As background information, we first describe one traditional, non-electrostatic device used for wavefront sensing. The *lenslet* array is a collection of tiny lenses of diameter 1 mm or smaller. Each lenslet intercepts one sector of the incoming wavefront and projects a focused spot onto a separate image plane. If the incoming wave is regular and planar, as in Fig. 1a, then the focused spots will be evenly spaced laterally across their common plane of focus. If, on the other hand, the wavefront is distorted, then any spots produced by lenslets that intercept deviant wavefronts will be displaced laterally, as in Fig. 1b. Spot displacement will be proportional to the amount by which the sector's wavefront deviates from being parallel to the image plane. In the language of adaptive optics, such a deviation is called wavefront *tilt*. When a lenslet array is used to measure wavefront tilt, the latter is measured in terms of lenslet spot displacement. Combining a lenslet array with a CCD camera and signal processing algorithm results in the Shack–Hartmann wavefront detector [2] widely used in adaptive optics.

A *deformable mirror* is a device whose reflective surface can be altered, sector by sector, to redirect the wavefronts of the incoming image. In an adaptive optics system, information derived from the wavefront sensor is used to control the slope of each sector of the deformable mirror's surface. As depicted schematically in Fig. 2, the deformable mirror changes the direction of propagation of each aberrant light ray from the incoming image until the wavefronts from the entire image are again parallel to the image plane. In essence, the aberrant wavefront sectors are redirected to their proper directions, thereby "undistorting" the distorted image. Examples of

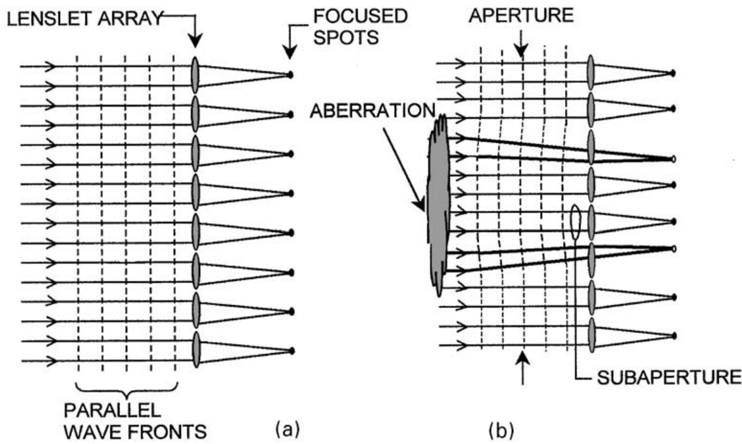

Fig. 1. (a) Lenslet array focusses parallel wave fronts in a uniform spot array. (b) Aberration in the optical path results in displacement of spots.

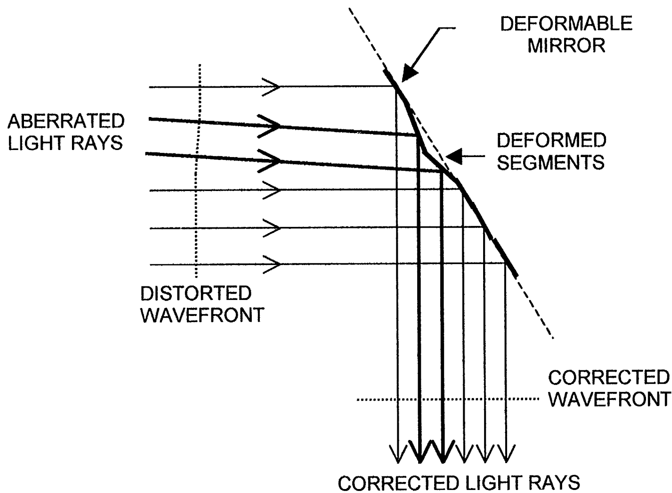

Fig. 2. Deformable mirror redirects aberrant rays of light.

continuously adjustable deformable mirrors include the single membrane OKO Technologies MEMS mirror [9–11] and the piston-actuated, continuous-membrane optical MEMS mirrors currently being developed at Boston University [12–16]. The Boston University mirrors, made from thin layers of polysilicon deposited over a silicon substrate, respond at mechanical frequencies exceeding 10 kHz for a 16×16 array of 250 μm actuators supporting a 2-mm square mirror surface. This feature makes real-time image correction possible in situations where the aberrations change rapidly with time. Examples include terrestrial imaging through turbulent air—for

example in a hot desert, astronomical imaging through the earth's atmosphere, medical imaging through airways or blood vessels, and point-to-point laser communications through smoke-filled, hazy, or turbulent air.

Real-time image correction that relies on a wavefront sensor of the lenslet type is computer-intensive and time-consuming and is often the primary source of bandwidth limitation in an adaptive-optics system. An analog-to-digital (A/D) converter must digitize the information from the CCD detector. A dedicated computer, microprocessor, or digital signal processing (DSP) chip must then decode the digitized data, sector by sector, to determine the positions of the lenslet spots, execute a control algorithm, and apply correction signals to the deformable mirror via a digital-to-analog (D/A) converter.

This paper proposes a novel way to perform sector wavefront sensing without the use of a lenslet array. A defining, proof-of-concept experiment has shown that the lenslet array can be replaced by a binary-actuated, electrostatic-actuated, digital-mirror device (DMD). The experiment reported here suggests that by incorporating a position-sensitive spot detector, analog processing circuit, and appropriate lenses, a system can be devised for performing subaperture wavefront sensing without the use of complicated digital image processing.

3. Digital mirror device

A DMD is an array of electrostatically-actuated micro-mirrors each capable of being driven into one of two fixed positions by the application of appropriate logic voltages. Unlike the sectors of the analog deformable mirrors used for wavefront correction, which are a continuously variable and interconnected as a single mirror membrane, the pixels of a DMD are not interconnected and reflect light in one of two preset directions only. Our experiments utilized the 600×800-element DMD that forms the core element of the Texas Instruments digital light processing video display system [17–20]. Each mirror pixel in the TI-DMD provides a $16\,\mu m \times 16\,\mu m$ reflective surface. As shown in the schematic view of Fig. 3, each mirror pixel has the shape of the letter "T" when viewed from the side. The top of the T is able to reflect light. The support system for the T acts as a restoring spring that, in the absence of other forces, causes the T to remain upright. Residual stresses and other fabrication variations in the support structure prevent the mirror surface from being perfectly horizontal when the T is at rest.

Electrostatic activation pads are placed beneath the two wings of the T. The T itself is electrically connected to ground via its own electrically-conductive support system. When a voltage is applied to the right-hand pad, as in the schematic view of Fig 4a, the resulting electrostatic attraction force causes the T to fully bend to the right until it reaches its mechanical limit with its mirror surface inclined at $+10^\circ$ to the horizontal. Similarly, when a voltage is applied to the left-hand pad, as in Fig. 4b, the T bends to the left until it reaches its other mechanical limit with the mirror inclined at -10°. These two deflection limits represent the logic **1** and logic **0** states of the mirror pixel, respectively.

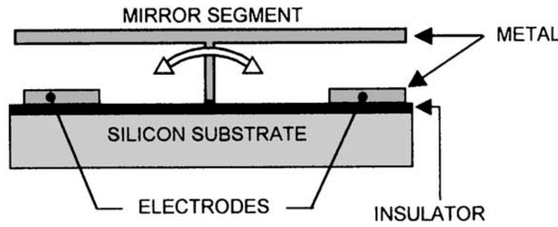

Fig. 3. Schematic view of single element of digital mirror device.

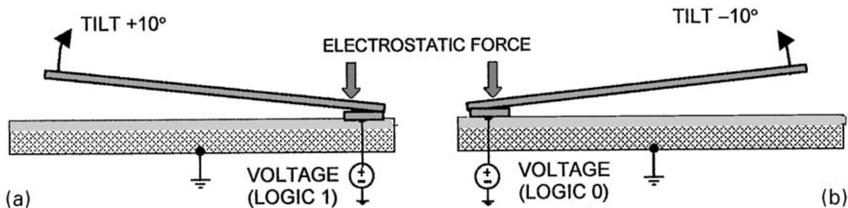

Fig. 4. Mirror pixel tilts $\pm 10^\circ$ in response to applied voltages. (a) Logic **1** voltage applied to right-hand electrode; "T" tilts to right. (b) Logic **0** voltage applied to left-hand electrode.

The individual mirror elements exhibit binary behavior because they are inherently unstable electromechanical devices. Although the mechanical behavior of the actual structure depicted schematically in Fig. 4 is complex, the magnitude of the restoring torque as a function of tilt angle can be expressed, to first order, as

$$T_{\mathrm{m}} = kr\theta. \tag{1}$$

Here θ is the tilt angle, T_{m} is the torque of mechanical origin, and k the torsional spring constant. For small tilt angles, the electrostatic force exerted on the tiltable mirror by either of the activation electrodes (with the unused electrode grounded) can be expressed as the change in stored electrostatic energy versus tilt angle:

$$F_{\mathrm{e}} = \frac{\mathrm{d}W}{\mathrm{d}\theta} = \frac{\mathrm{d}}{\mathrm{d}\theta}\frac{CV^2}{2} = \frac{V^2}{2}\frac{\mathrm{d}}{\mathrm{d}\theta}\frac{\varepsilon A}{(g - r\theta)} = \frac{\varepsilon A r}{2}\frac{V^2}{(g - r\theta)^2}. \tag{2}$$

Here W is the stored electrostatic energy, V the applied voltage, A the area of the actuation electrode, g the electrode-to-mirror gap at zero tilt, r the average turning radius of the T-shaped structure, and θ the mirror tilt angle. An approximate value for the capacitance C is found by dividing A by the quantity $(g - r\theta)$, where $r\theta$ is the reduction in gap spacing due to the tilting of the "T" by an angle θ.

The torque T_{e} exerted on the mirror will be equal to F_{e} multiplied by r. Eq. (2) varies as the square hyperbolic of tilt angle θ and is parabolic in voltage V. Fig. 5 shows superimposed plots of T_{e} and T_{m} for various values of voltage. In plotting these theoretical curves, reasonable estimates have been made for $kr = 1.5 \times 10^{-9}\,\mathrm{N\,m/rad}$, $A = 12 \times 10^{-12}\,\mathrm{m}^2$, $g = 4\,\mu\mathrm{m}$, and $r = 8\,\mu\mathrm{m}$. As is evident in this plot, for small voltages the mirror reaches a deflection equilibrium where

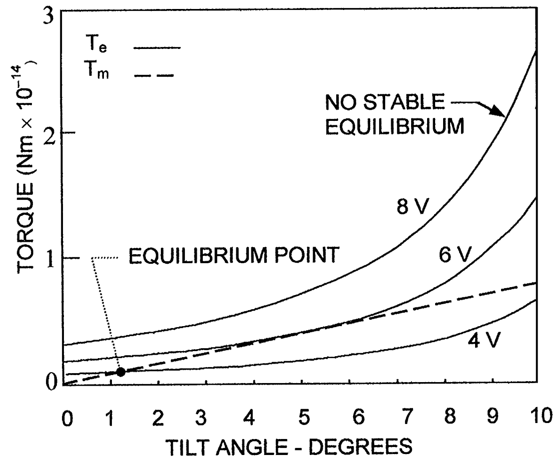

Fig. 5. Plots of mechanical restoring torque T_m versus electrostatic torque T_e for various values of applied voltage.

$T_m = T_e$ for some small angle θ. For larger voltages, the electrostatic and mechanical torques do not balance for any value of θ. This lack of stable equilibrium is the defining characteristic of digital MEMS devices. The TI-DMD is operated as a digital MEMS device wherein the binary positions of each mirror pixel are determined by the $+10^\circ$ mechanical deflection limits of the mirror, rather than by the exact value of applied voltage. Because the geometry of the physical structure can be controlled more reliably than the mechanical restoring force, a digital device is appropriate for a system where the angles of light reflection are critical.

A detailed drawing of the actual TI-DMD mirror structure is shown in Fig. 6. This complex device has the same basic function as that depicted in Fig. 4. A scanning electron micrograph showing clusters of pixels in their $+10^\circ$ and -10° positions is shown in Fig. 7. The mechanical bandwidth of these devices is reported to be up to 60 kHz.

4. Setup for proof-of-concept experiments

In the work reported in this paper, a TI-DMD replaced the traditional lenslet array in a Shack–Hartmann imaging system. The pixels of the DMD define the subapertures of the image plane for the purpose of wavefront detection. The experiments reported here were designed to prove that the DMD can replace the lenslet array as the subaperturing device in an adaptive-optics imaging system. In the control version of the experiment, depicted in Fig. 8a, an expanded, collimated laser beam was directed onto a fixed, planar, front-surfaced mirror and passed through a 1048 element array of 250-μm diameter lenslets before landing on the image plane of a CCD detector. In an alternative version of the experiment, depicted in Fig. 8b, the

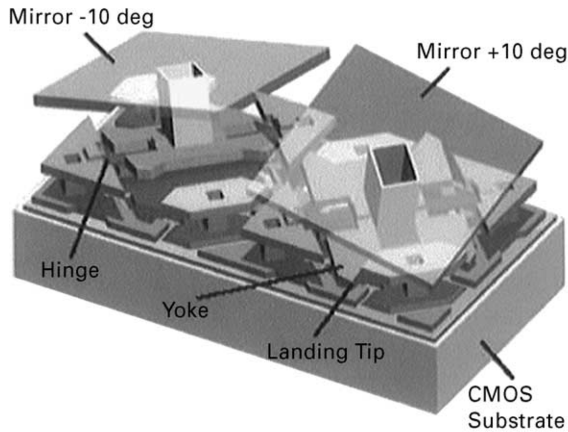

Fig. 6. Structural details of two pixels of the TI-DMD. Mirror size is 16 μm × 16 μm. (Courtesy of Texas Instruments.)

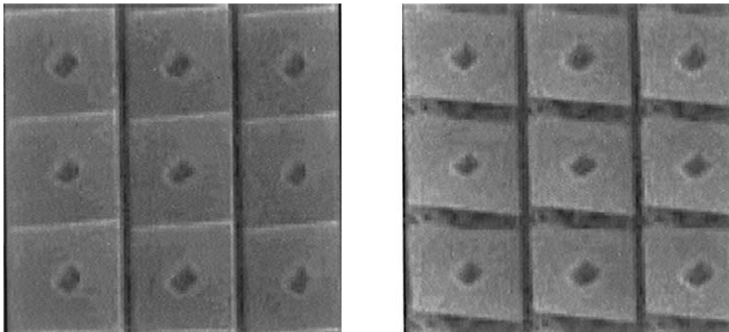

Fig. 7. Scanning electron micrographs of pixel clusters of the TI-DMD. Left: $-10°$; right: $10°$. (Courtesy of Texas Instruments.)

lenslet array was replaced by a digital mirror device. Various subgroups of adjacent DMD pixels were used to define subsections of the image plane. These subsections were chosen to correspond to exactly the same image plane subsections intercepted by each individual lens in the lenslet array. The pixels within each DMD subsection could be forced to either their "on" (logic **1**) positions, thereby reflecting light onto the image plane of the CCD for processing, or to their "off" (logic **0**) positions, thereby causing their light to deflect out of the optical path and completely away from the CCD.

Fig. 9 shows a 12-spot subset of the CCD image produced by the lenslet array. Fig. 10 shows the corresponding CCD image produced when the laser beam reflected off a 3 × 4 array of 240-μm × 240-μm DMD pixel clusters corresponding to the same

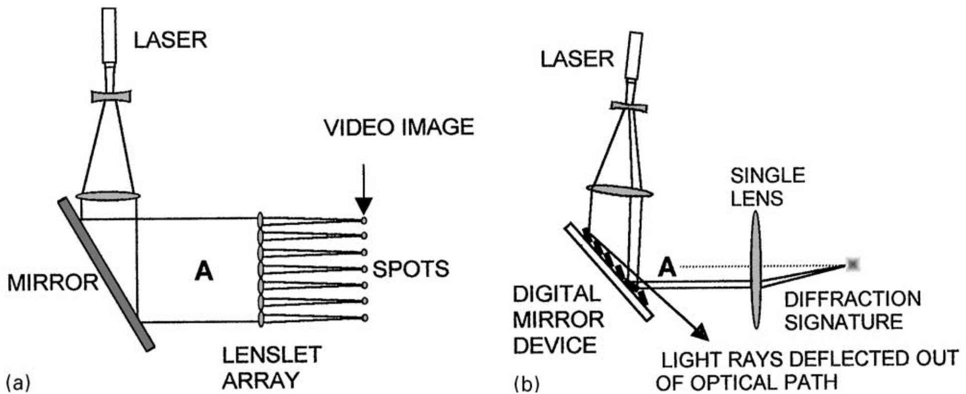

Fig. 8. (a) Conventional lenslet array used as a subaperturing device; (b) digital mirror device replaces the lenslet array.

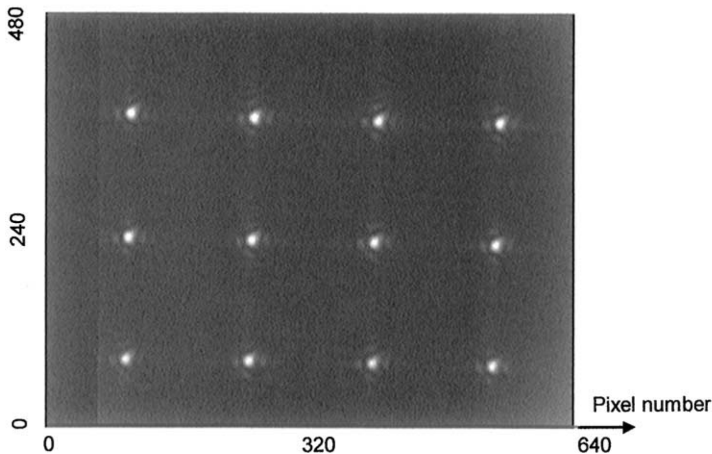

Fig. 9. A 3×4 spot subset of the CCD image produced by a 1048-element array of 250-μm lenslets.

subapertures as the lenslet array. As can be seen in Fig. 10, the light reflected from the DMD pixel clusters does not produce focused spots, but rather small, identifiable diffraction patterns generated by the irregular surface presented by the clusters of "on" mirror pixels. This image pattern also exhibits considerable two-dimensional diffraction, as expected for a square aperture.

In both versions of the experiment depicted in Fig. 8, a fixed, controlled aberration consisting of a 1-mm thick, bent microscope slide was next introduced into the optical path at point A. The digitized image from the CCD was stored in a computer, and an image processing algorithm, written in MATLAB™, was used to determine the location of the focused lenslet spots and of the centroids of the diffraction patterns from the TI-DMD.

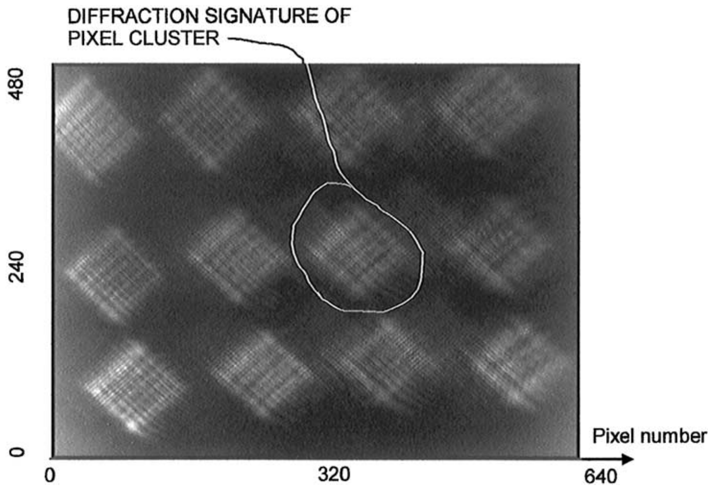

Fig. 10. Diffraction signature of 3×4 cluster of DMD mirror pixels.

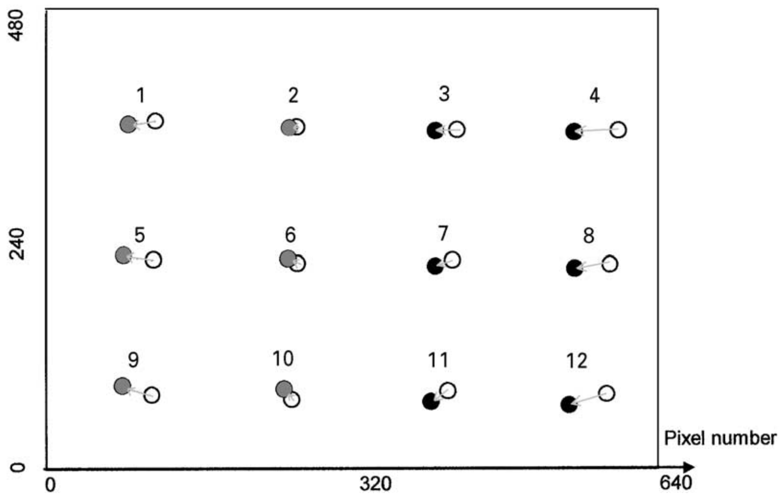

Fig. 11. Spot positions from a 3×4 subset of lenslets both with (black) and without (white) an aberration in the optical path. Arrows indicate the dot displacements caused by the aberration.

5. Results

A reproduction of the superimposed images from a 3×4 group of lenslet spots is shown in Fig. 11. These spot positions were taken from actual CCD images of the type shown in Fig. 9 but are reproduced here as a line drawing for clarity. The vectors point from the unaberrated spots to the aberrated spots.

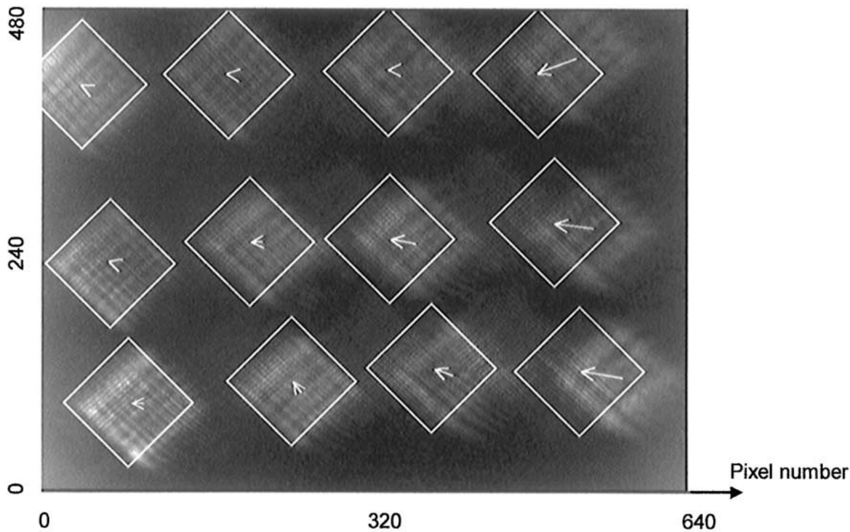

Fig. 12. Diffraction signature patterns of TI-DMD pixel clusters with and without optical path aberrations. The white outlines indicate the displacements of the signature patterns when the aberration is in place and the arrow indicate the amount of signature displacement.

The same system was used to determine the shifts in location of the TI-DMD sector diffraction patterns. Fig. 12 shows the superimposed images of the patterns from a 3×4 set of 250-μm DMD pixel clusters both with and without the aberration in place. These subapertures represent the same image plane subapertures defined by the 3×4 group of lenslets in Fig. 9.

Fig. 13 shows the x-components of displacement indicated in Figs. 11 and 12 as measured by an image detection algorithm. The x-components of the TI-DMD displacement vectors have been multiplied by a scaling factor of 2. This figure suggests that the displacements measured using the TI-DMD system are proportional to those obtained from the lenslet wavefront sensor. A similar trend can be seen with respect to the y-components of the displacement vectors.

6. Conclusion

The ability of an electrostatic, binary-activated DMD to isolate a solitary subaperture on demand provides great freedom to the designer of an adaptive-optics system. Small subapertures of the incoming image can be isolated and focused to a common location where a single, position-sensitive sensor is placed. Such a system would permit a sequential correction method that could replace the more traditional and complex adaptive optics scheme involving a lenslet array and digital signal processing system. One example of position-sensitive spot sensors is the quad-cell photodetector. This device consists of four pie-shaped semiconductor sensors mounted within the same package. When the quad-cell detector is connected to

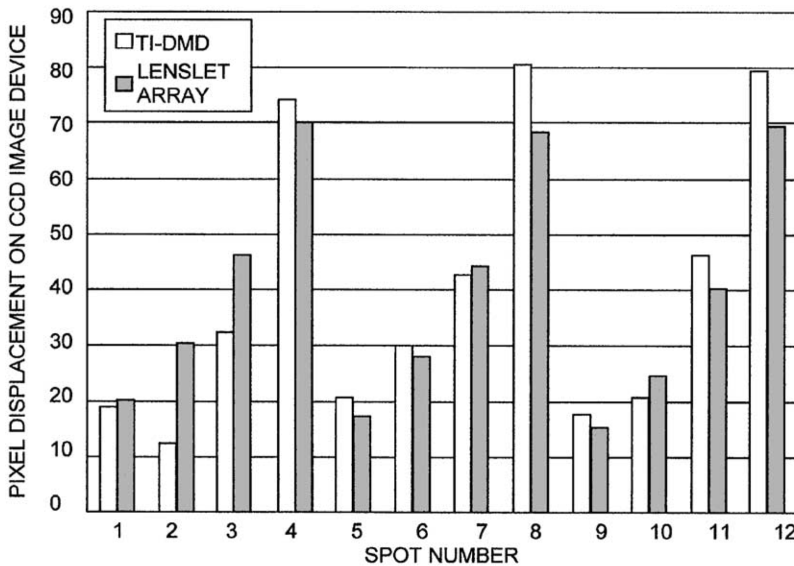

Fig. 13. Magnitude of x-axis displacements of lenslet spots (gray) and TI-DMD diffraction signatures (white) versus spot number. Relative displacements are measured in units of pixels on the CCD imaging device.

appropriate electronics, it produces two analog signals that indicate the x- and y-axis deviation of the focused image from the center of the detector. Each subaperture of the image field in an adaptive optics system may thus be turned on in sequence and the analog output from the photodetector used to control the corresponding segment of the deformable correction mirror. This correction can take place without requiring the signal from the photodetector to be digitized and processed by a computer. This latter step is a very time-consuming one in a traditional adaptive-optics system. The serial subaperturing capability of a digital mirror device allows the system to isolate many small regions of the wavefront and direct them to a single, position-sensitive detector. Such a system could facilitate a sequential correction method that could replace the more complex schemes used in traditional adaptive optics.

References

[1] P. Wizinowich, B. McLeod, M. Lloyd-Hart, R. Angel, D. Colucci, R. Dekany, D. McCarthy, D. Wittman, I. Scott-Fleming, Adaptive optics for array telescopes using piston and tilt wavefront sensing, Appl. Opt. 31 (1992) 6036–6046.

[2] B.M. Welsh, B.L. Ellerbroek, M.C. Roggemann, T.L. Pennington, Fundamental performance comparison of a Hartmann and a shearing interferometer wavefront sensor, Appl. Opt. 34 (1995) 4186–4195.

[3] R.Q. Fugate, W.J. Wild, Untwinkling the stars—part 1, Sky and Telescope, 24–31, May 1994.

[4] G.D. Love, Wavefront correction and production of Zernike modes with a liquid crystal SLM, Appl. Opt. 36 (1997) 1517–1524.
[5] J. Gourlay, G.D. Love, P.M. Birch, R.M. Sharples, A. Purvis, Areal-time closed-loop liquid crystal adaptive optics system: first results, Opt. Commun. 137 (1997) 17–21.
[6] A. Kudryashov, J. Gonglewski, S. Browne, R. Highland, Liquid crystal phase modulator for adaptive optics: Temporal performance characterization, Opt. Commun. 141 (1997) 247–253.
[7] J. Gonglewski, S. Brown, S. Rogers, S. McDermott, Adaptive optics using a liquid crystal phase modulator in conjunction with a Shack–Hartmann wave-front sensor and zonal control algorithm, Opt. Express 1 (11) (1997) 338.
[8] K.H. Brenner, M. Kufner, S. Kufner, J. Moisel, A. Müller, S. Sinzinger, M. Testorf, J. Göttert, J. Morf, Application of three-dimensional micro-optical components formed by lithography, electroforming, and plastic molding, Appl. Opt. 32 (1993) 6464–6469.
[9] L.M. Miller, M.L. Argonin, R.K. Bartman, W.J. Kaiser, T.W. Kenny, R.L. Norton, E.C. Vote, Fabrication and characterization of micromachined deformable mirror for adaptive optics applications, Proceedings of the SPIE, Vol. 1954, 1993, pp. 421–430.
[10] G.V. Vdovin, S. Middelhoek, M. Bartek, P.M. Sarro, D. Solomatine, Technology, characterization and applications of adaptive mirrors fabricated with IC-compatible micromachining, Proceedings on Adaptive Optical Systems and Applications, Vol. SPIE 2534, 1995, pp. 116–129.
[11] G.V. Vdovin, P.M. Sarro, Flexible mirror micromachined in silicon, Appl. Opt. 34 (1995) 2968–2972.
[12] M.N. Horenstein, T.G. Bifano, S. Pappas, J. Perreault, R. Krishnamoorthy-Mali, Real-time optical correction using electrostatically actuated MEMS devices, J. Electrostat. 46 (1999) 91–101.
[13] T. Bifano, J. Perreault, R.K. Mali, M.N. Horenstein, Microelectromechanical deformable mirrors, J. Selected Topics Quant. Electron. 5 (1) (1999) 83–89.
[14] M.N. Horenstein, T.G. Bifano, R. Krishnamoorthy, N. Vandelli, Electrostatic effects in micromachined actuators for adaptive optics, J. Electrostat. 42 (1–2) (1997) 69–82.
[15] T.G. Bifano, R. Krishnamoorthy-Mali, J.K. Dorton, J. Perreault, N. Vandelli, M.N. Horenstein, D.A. Castanon, Continuous membrane surface micromachined silicon deformable mirror, Opt. Eng. 36 (5) (1997) 1354–1360.
[16] R. Mali, T. Bifano, N. Vandelli, M. Horenstein, Development of microelectromechanical deformable mirrors for phase modulation of light, Opt. Eng. 36 (2) (1997).
[17] L.J. Hornbeck, Deformable-mirror spatial light modulators, in: Spatial Light Modulators and Applications III—SPIE Critical Reviews, Vol. 1150, 1989, pp. 86-102.
[18] J.B. Sampsell, An overview of Texas Instruments digital micromirror device (DMD) and its application to projection displays, Society for Information Display International Symposium on Digest of Technical Papers, Vol. 24, 1993, pp. 1012–1015.
[19] M.A. Mignardi, Digital micromirror array for projection TV, Solid State Technol. 37 (1994) 63–66.
[20] Texas Instruments DLP: Creating Dramatic Visual Experiences Through Digital Imaging, http://www.ti.com/dlp.